

Chimeras confined by fractal boundaries in the complex plane

Cite as: Chaos **31**, 053104 (2021); <https://doi.org/10.1063/5.0049631>

Submitted: 07 March 2021 . Accepted: 16 April 2021 . Published Online: 03 May 2021

 Ralph G. Andrzejak

COLLECTIONS

Paper published as part of the special topic on [In Memory of Vadim S. Anishchenko: Statistical Physics and Nonlinear Dynamics of Complex Systems](#)



View Online



Export Citation



CrossMark

ARTICLES YOU MAY BE INTERESTED IN

[Dynamics of a fractional epidemiological model with disease infection in both the populations](#)

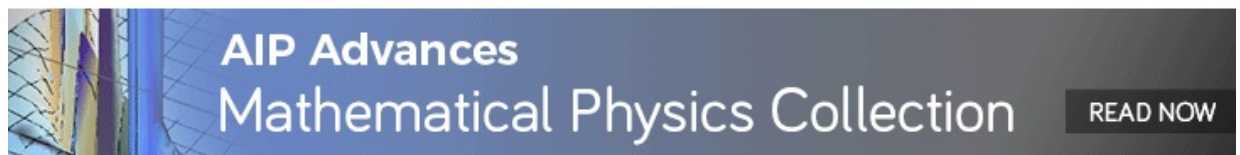
Chaos: An Interdisciplinary Journal of Nonlinear Science **31**, 043130 (2021); <https://doi.org/10.1063/5.0028905>

[Phase coalescence in a population of heterogeneous Kuramoto oscillators](#)

Chaos: An Interdisciplinary Journal of Nonlinear Science **31**, 041104 (2021); <https://doi.org/10.1063/5.0050451>

[Quasi-objective coherent structure diagnostics from single trajectories](#)

Chaos: An Interdisciplinary Journal of Nonlinear Science **31**, 043131 (2021); <https://doi.org/10.1063/5.0044151>



AIP Advances
Mathematical Physics Collection

READ NOW



Chimeras confined by fractal boundaries in the complex plane

Cite as: Chaos 31, 053104 (2021); doi: 10.1063/5.0049631

Submitted: 7 March 2021 · Accepted: 16 April 2021 ·

Published Online: 3 May 2021



View Online



Export Citation



CrossMark

Ralph G. Andrzejak^{a)} 

AFFILIATIONS

Department of Information and Communication Technologies, Universitat Pompeu Fabra, 08018 Barcelona, Catalonia, Spain

Note: This paper is part of the Focus Issue, In Memory of Vadim S. Anishchenko: Statistical Physics and Nonlinear Dynamics of Complex Systems.

^{a)}Author to whom correspondence should be addressed: ralph.andrzejak@upf.edu

ABSTRACT

Complex-valued quadratic maps either converge to fixed points, enter into periodic cycles, show aperiodic behavior, or diverge to infinity. Which of these scenarios takes place depends on the map's complex-valued parameter c and the initial conditions. The Mandelbrot set is defined by the set of c values for which the map remains bounded when initiated at the origin of the complex plane. In this study, we analyze the dynamics of a coupled network of two pairs of two quadratic maps in dependence on the parameter c . Across the four maps, c is kept the same whereby the maps are identical. In analogy to the behavior of individual maps, the network iterates either diverge to infinity or remain bounded. The bounded solutions settle into different stable states, including full synchronization and desynchronization of all maps. Furthermore, symmetric partially synchronized states of within-pair synchronization and across-pair synchronization as well as a symmetry broken chimera state are found. The boundaries between bounded and divergent solutions in the domain of c are fractals showing a rich variety of intriguingly esthetic patterns. Moreover, the set of bounded solutions is divided into countless subsets throughout all length scales in the complex plane. Each individual subset contains only one state of synchronization and is enclosed within fractal boundaries by c values leading to divergence.

Published under an exclusive license by AIP Publishing. <https://doi.org/10.1063/5.0049631>

This work is dedicated to the late Vadim Anishchenko. His landmark papers on maps and on chimera states in networks of coupled maps^{1–18} represent only one branch in his plentiful contributions to the fields of nonlinear dynamics of deterministic and stochastic systems. Chimera states are characterized by the coexistence of synchronization and desynchronization in networks of coupled dynamics.^{19,20} The set of initial conditions leading to chimera states can form riddled and fractal basins of attraction.^{21–23} Initial conditions outside of these basins of attraction can result in fully synchronized or fully desynchronized dynamics, among others. While chimera states were first described¹⁹ and continue to be studied for networks of time-continuous oscillators, an increasing interest is paid to networks of time-discrete maps. Chimera states were found for networks of coupled logistic maps,^{4–8,9,23–31} Henon maps,^{10–15,21} cubic maps,^{7,16,17} map-based neuron models,^{18,32} sine-circle maps,^{33–35} sine-squared maps,^{23,26,36} cosine maps,³⁷ piecewise linear maps,³⁸ and piecewise logistic maps.³⁸ Recently, two populations of quadratic maps with real-valued parameter c were shown to yield

a plentitude of dynamics including chimera states.³⁹ Quadratic maps, however, reveal their full complexity only for complex-valued parameters c . In particular, they allow one to generate fractal Julia sets and Mandelbrot sets in the complex plane.^{40–44} Our aim here is to explore this complexity without adding the complicatedness of a high-dimensional network. We, therefore, study a minimal two-population network of two pairs of two quadratic maps with complex-valued parameters c . We use non-random initial conditions defined by the first four iterates of uncoupled quadratic maps. Our results show that in dependence on c , the network iterates can diverge to infinity or remain bounded, and that bounded solutions can get fully synchronized, fully desynchronized, or enter into some partially synchronized state, including a symmetry broken chimera state. The boundaries between these different states in the domain of the complex-valued c form fractal patterns. In contrast to the high-dimensional fractal basins of attraction,^{21–23} these fractals reside in the complex plane and are, therefore, straightforward to visualize. In qualitative terms, the fractals generated by our network

of coupled quadratic maps seem less filigree, more disordered, but even fuller of variety than the Mandelbrot set. Complementing previous work,^{21–23} our study establishes an intriguing link between the dynamics of partially synchronized networks and the geometry of fractals in the complex plane.

I. INTRODUCTION

We use the quadratic map $f_c(z_{n+1}) = z_n^2 + c$, where n is the discrete time in units of the iteration step, and c is a complex-valued parameter. The complex-valued iterates of f_c either remain bounded for all times n or diverge to infinity. Whether or not the iterates diverge depends on the parameter c and the initial condition z_0 . Given f_c and a certain c , the Julia set is defined by the boundary between the complex-valued initial conditions for which f_c diverges and the ones for which it remains bounded.^{40,41} If and only if the origin of the complex plane $z_0 = 0$ belongs to the initial conditions, which lead to bounded behavior of f_c , the Julia set is connected. Otherwise, the Julia set is a Cantor space. The Mandelbrot set is defined by the set of c for which the Julia set is connected, or equivalently, by the set of c for which iterates z_n of f_c initiated at $z_0 = 0$ remain bounded for all n .^{42–44}

We have shown previously that two identical populations of quadratic maps f_c yield a plentitude of dynamics, which can be symmetric or symmetry broken with regard to the two populations.³⁹

In particular, these dynamics included chimera states for which one population was identically synchronized while the other remained incoherent. However, in this previous work, we only considered real-valued parameters c and initial conditions, such that the dynamics of the populations remained in the real-valued domain. What type of dynamics can arise if complex-valued parameters c are used? To address this question, we here analyze a coupled network F_c of two pairs, each composed by two quadratic maps f_c , which is the smallest network that allows us to study synchronization within and across pairs of maps. This parsimonious approach to use a minimal two-population network of only two maps per population is different from Ref. 39, where each population consisted of 100 maps. For previous work on chimera states in networks consisting of a minimal number of nodes, see, for example, Refs. 45–52.

II. A MINIMAL TWO-POPULATION MODEL

The map f_c is governed by a sole parameter c , which is set to be the same for all four maps of the network F_c . Hence, all maps of F_c are identical. Each map is coupled with strength C_w to the other map within its own pair and with strength C_a to the two maps in the other pair. The maps of the first pair are called U_c and V_c , and the ones of the second pair are called P_c and Q_c . Accordingly, F_c can be written as

$$U_c: u_{n+1} = f_c(u_n) + C_w \cdot [f_c(v_n) - f_c(u_n)] + C_a \cdot [(f_c(p_n) - f_c(u_n)) + (f_c(q_n) - f_c(u_n))], \quad (1)$$

$$V_c: v_{n+1} = f_c(v_n) + C_w \cdot [f_c(u_n) - f_c(v_n)] + C_a \cdot [(f_c(p_n) - f_c(v_n)) + (f_c(q_n) - f_c(v_n))], \quad (2)$$

$$P_c: p_{n+1} = f_c(p_n) + C_w \cdot [f_c(q_n) - f_c(p_n)] + C_a \cdot [(f_c(u_n) - f_c(p_n)) + (f_c(v_n) - f_c(p_n))], \quad (3)$$

$$Q_c: q_{n+1} = f_c(q_n) + C_w \cdot [f_c(p_n) - f_c(q_n)] + C_a \cdot [(f_c(u_n) - f_c(q_n)) + (f_c(v_n) - f_c(q_n))]. \quad (4)$$

Equations (1)–(4) are the usual equations for two populations of coupled maps. For such a small network, we can use a different symbol for each map instead of indices, which allows us to simplify the notation below. We study F_c in dependence on the parameter c for the following non-random initial conditions. For every value of c , we calculate the first four iterates of the individual quadratic map f_c started at $z_0 = 0$. These values are then used as initial conditions of the four coupled maps: $u_0 = z_1$, $v_0 = z_2$, $p_0 = z_3$, and $q_0 = z_4$. Therefore, except for c values for which f_c directly enters into a fixed point, period-2 or period-3 cycle, the network is always initialized in a fully asynchronous state at time $n = 0$. We run the network for a total of $n_{\max} = 5 \times 10^5$ iterations. This choice of n_{\max} and why we do not use random initial conditions is discussed in detail below. Unless stated otherwise, the coupling strengths are fixed at $C_w = 0.01$ and $C_a = 0.0025$. These parameters are set such that the coupling within pairs is stronger than the one across pairs. Beyond this constraint, the exact values of C_w and C_a are not tuned in any way.

If for a certain c , the maps leave the range of floating point numbers, we determine the onset of this divergence by $n_{\text{div}} = \min \{n \mid \max\{|u_n|, |v_n|, |p_n|, |q_n|\} > 2\}$, where $|\cdot|$ denotes the absolute value in the complex plane. This threshold is arbitrary, and the particular value of 2 is taken over from the point-of-no-return criterion of individual maps f_c (see also Sec. VI). For all bounded solutions, we use the following criteria to test for synchronization between all six pairings of maps and to determine if the maps have entered into a periodic cycle. To detect synchronization between the maps U_c and V_c , we use the criterion $|u_{n_{\max}} - v_{n_{\max}}| < \varepsilon_{\text{NUM}} = 10^{-13}$, which corresponds to identical synchronization within the limits of numerical precision.⁵³ We write $U_c = V_c$ to indicate that U_c and V_c are synchronized, and $U_c \neq V_c$ to indicate that they are not. The same criterion and analogous notations are used for all five remaining pairings of maps. To detect a period- m cycle of the map U_c , we use the criterion $|u_{n_{\max}} - u_{n_{\max}-m}| < \varepsilon_{\text{NUM}}$, and analogously for V_c , P_c , and Q_c . We never observed dynamics for which the

different maps were in periodic cycles of different lengths. Accordingly, we directly refer to a period- m cycle of the network F_c . A fixed point of F_c corresponds to $m = 1$.

III. THE DYNAMICS IN THE COMPLEX DOMAIN OF THE NETWORK ITERATES

Figure 1 shows the dynamics of F_c obtained for eight exemplary c values. We denote these values by $c_{1,\dots,8}$ and list them in Table II in the Appendix. In the first example [c_1 , Fig. 1(a)], the four maps undergo different transient states each, but then they all converge to the same fixed point, i.e., we get $U_c = V_c = P_c = Q_c$. We also obtain this full synchronization of all maps for c_2 [Fig. 1(b)]. However, in this case, the maps do not converge to a fixed point but jointly enter into a period-3 cycle. Also, in the third example [c_3 , Fig. 1(c)], F_c enters into a period-3 cycle. In contrast to the first two examples, however, synchronization is found within the two pairs but not across them. That means we get within-pair synchronization, $U_c = V_c \neq P_c = Q_c$. A chimera state is established in

the fourth example [c_4 , Fig. 1(d)]. While the first pair synchronizes ($U_c = V_c$), the maps of the second pair enter into distinct cycles and remain unsynchronized among them ($P_c \neq Q_c$) and also from the synchronized pair ($P_c \neq U_c = V_c \neq Q_c$). A somewhat counter-intuitive result is obtained in the next example [c_5 , Fig. 1(e)]. Here, the maps do not synchronize within populations but across populations. All maps at first follow their respective transient motions. For example, the iterates of V_c initially fill three ring-shaped structures in an aperiodic way. Then, at $n \approx 4760$, the dynamics reorganizes abruptly. The map V_c is driven away from its initial ring-shaped transients and then re-injected to the center of the overall dynamics. Instead of returning to the initial ring-shaped structures, it then synchronizes with P_c . Furthermore, U_c and Q_c synchronize across pairs. Overall, we get $U_c = Q_c \neq V_c = P_c$, i.e., across-pair synchronization instead of within-pair synchronization. In the sixth example [c_6 , Fig. 1(f)], none of the maps synchronize. Instead, each map enters into a distinct period-3 cycle. Inspecting the spatial distribution of the three different symbols that represent the phase of the maps within their respective cycle, we see that maps follow similar

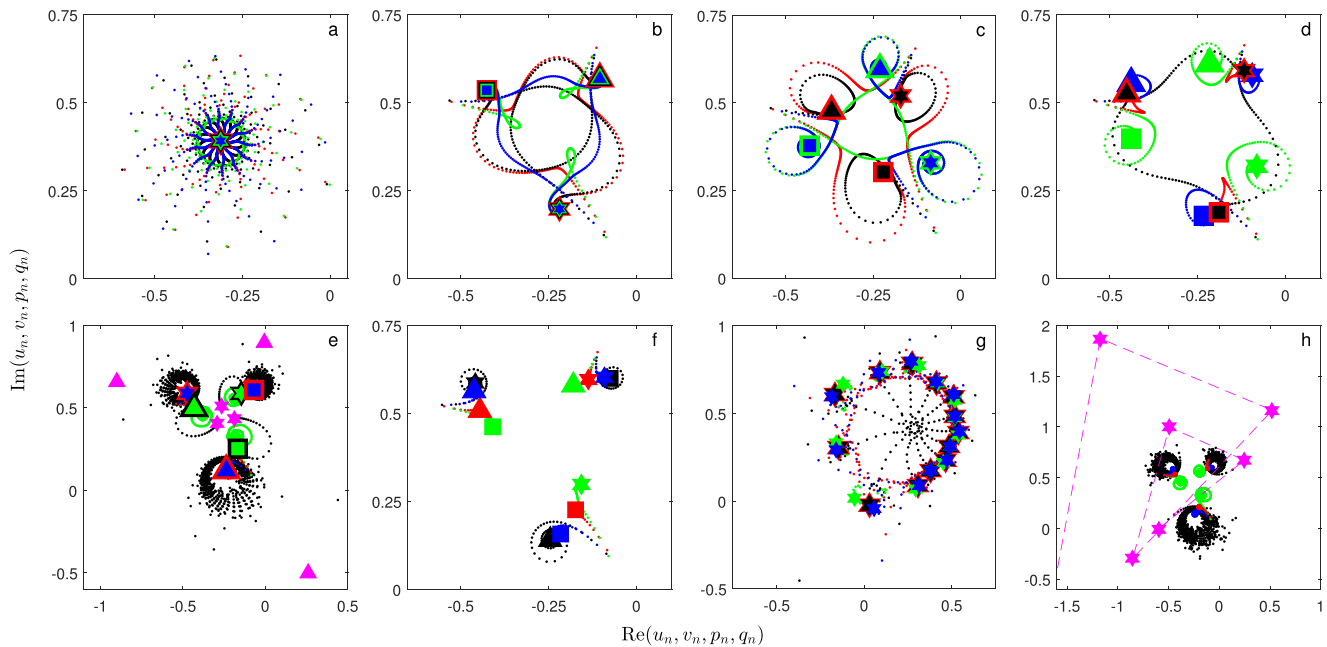


FIG. 1. Different values of c lead to qualitatively different dynamics of the network of four coupled maps F_c . Iterates u_n (red), v_n (black), p_n (green), and q_n (blue) obtained for eight exemplary values $c_{1,\dots,8}$, listed in Table II in the Appendix. (a) Results for c_1 . At $n = 18\,599$, all four maps have converged to a joint fixed point. Small dots: iterates during initial transients, $n = 1, \dots, 18\,598$. Stars: $u_n = v_n = p_n = q_n$ for $n \geq 18\,599$. Stars of different sizes allow all overlaid symbols to be seen. Panel (b) is analogous to panel (a) but for c_2 . Here, convergence to $u_n = v_n = p_n = q_n$ is reached at $n = 1487$. Additional symbols are used because the maps converge to a period-3 cycle. Triangles: $n = 1487, 1490, \dots$; squares: $n = 1488, 1491, \dots$; stars $n = 1489, 1492, \dots$ (c) For c_3 , convergence to $u_n = v_n$ and $p_n = q_n$ is reached at $n = 6299$. Symbols continue to indicate the different phases of the period-3 cycles. Since the maps synchronize within pairs but not across pairs, only the red and black as well as the blue and green symbols are overlaid. (d) Convergence to the chimera state of $u_n = v_n$ and $p_n \neq q_n$ is reached at $n = 2318$ for c_4 . (e) For c_5 convergence to $u_n = q_n$ and $v_n = p_n$ is reached at $n = 6175$. Additional magenta symbols serve to highlight the abrupt reorganization of the dynamics. Magenta triangles: u_n for $n = 4758, 4759, 4760$; magenta stars: u_n for $n = 4761, 4762, 4763$. (f) For c_6 , convergence is attained at $n = 2934$. Here, all maps converge to a distinct period-3 cycle such that no symbols are overlaid. (g) Like for c_4 in panel (d), for c_7 the dynamics converges to $u_n = v_n$ and $p_n \neq q_n$, here at $n = 1749$. Instead of a period-3 cycle, we find a period-13 cycle. Stars depict all 13 phases of these cycles, which are visited clock-wise advancing two positions per iteration such that after 13 iterations the ring-shaped structure is circumscribed twice. (h) For c_8 , the dynamics does not settle to any bounded solution but diverges toward infinity. Magenta stars connected by lines show the iterates u_n for $n = 8336, \dots, 8341$. The iterate u_{8342} is already outside of the displayed range. Ten iterations later u_n, v_n, p_n, q_n will all have left the range of floating point numbers.

TABLE I. Five states of synchronization illustrated in Figs. 1(a)–1(g). The penultimate column indicates the panels of Fig. 1, which contain the corresponding examples. The last column specifies the colors used to represent the states in Figs. 3–6(a). Recall that we use the equality sign to indicate that the maps are identically synchronized within the limits of numerical precision.

Type	Description	Formula	Example in Fig. 1	Color in Figs. 3–6(a)
Full synchronization	All maps synchronized	$U_c = V_c = P_c = Q_c$	(a), (b)	Blue
Within-pair synchronization	Maps synchronized within pairs but desynchronized across pairs	$U_c = V_c \neq P_c = Q_c$	(c)	Yellow
Across-pair synchronization	Maps synchronized across pairs but desynchronized within pairs	$U_c = P_c \neq V_c = Q_c$ or $U_c = Q_c \neq V_c = P_c$	(e)	Green
Chimera state	Maps synchronized in one pair but desynchronized in the other pair	$U_c = V_c$ but $P_c \neq Q_c$ or $P_c = Q_c$ but $U_c \neq V_c$	(d), (g)	Purple
Full desynchronization	All pairings of maps desynchronized	$U_c \neq V_c, V_c \neq P_c, P_c \neq Q_c, Q_c \neq U_c,$ $Q_c \neq V_c, P_c \neq U_c$	(f)	Red

cycles but with a relative lag to each other. This lag becomes most evident for the example of c_6 , but can also be seen for c_4 and c_5 . In the examples discussed so far, we used a fixed point in Fig. 1(a) and period-3 cycles in Figs. 1(b)–1(f) simply for ease of readability of these figures. However, all states of synchronization can also be attained for higher order periods, as illustrated by a chimera state of period 13 [c_7 , Fig. 1(g)]. Like in the fourth example in Fig. 1(d), the pair U_c and V_c synchronizes identically, while the maps of the pair P_c and Q_c enter into distinct cycles and remain unsynchronized. The five different states of synchronization seen in the examples of Figs. 1(a)–1(g) are summarized in Table I.

The parameter value used for the last example c_8 in Fig. 1(h) is obtained by only slightly changing c_5 . Both values differ by 10^{-7} in their imaginary part (see again Table II in the Appendix). As a result of the smallness of this change, the initial transients obtained for c_8 look similar to those obtained for c_5 . However, eventually a different outcome is obtained. At $n \approx 8340$ the map V_c gets carried away from its initial ring-shaped transients. This is similar to what happens for c_5 after approximately 4750 iterations. However, for c_8 , the iterates of V_c are not re-injected to the center of the overall dynamics but diverge toward infinity instead. As a consequence of the coupling also the other maps get carried away toward infinity. By the time of iteration $n = 8352$, the iterates of all maps have left the range of floating point numbers. In contrast to all previous examples $c_{1,\dots,7}$, the network F_c diverges for c_8 . Hence, the dichotomous behavior of f_c , of either remaining bounded or diverging, carries over to our network of four coupled maps F_c .

We can now relate the value of n_{\max} fixed above to the length of the transients observed in Fig. 1. The network F_c always undergoes transients before converging to some final bounded state or diverging to infinity. We, therefore, have to estimate the number of iterations for which we can assume that F_c has settled to its asymptotic dynamics. The problem is that the length of the transients depends on c . Any bounded or divergent dynamics can be preceded by short or long transients. Moreover, for some c values, the transients can be longer than times accessible for numerical simulations. Being aware of this unavoidable limitation, we determined in pre-analysis that the value $n_{\max} = 5 \times 10^5$ leads to a sufficient precision throughout all ranges of c we consider below.

IV. MAPPING THE ASYMPTOTIC DYNAMICS IN THE COMPLEX DOMAIN OF THE PARAMETER c

Results of Fig. 1 show that different values of c can lead to qualitatively different dynamics of F_c . Even an arbitrarily small difference in c can be decisive for the outcome [see again Fig. 1(e) vs Fig. 1(h)]. What results are obtained when we vary c quasi-continuously in the complex plane? To address this question, we look at mappings of bounded vs divergent behavior of F_c . In analogy to the definition of the Mandelbrot set, we define \mathcal{A} by the set of c values for which the network F_c shows bounded behavior [such as in Figs. 1(a)–1(g)]. The complement of \mathcal{A} is called \mathcal{B} . In other words, \mathcal{B} is the set of c for which the network shows divergent behavior [such as in Fig. 1(h)]. The set \mathcal{A} is divided further into subsets with regard to the different periodic cycles or the different states of synchronization attained by the iterates of F_c as a function of c .

Figures 2(a) and 2(b) allow comparing the macroscopic shape of \mathcal{A} to the one of the Mandelbrot set and inspecting the division of both sets with regard to the periodic cycles of the respective dynamics F_c and f_c . While alterations can be seen in the peripheral structure, \mathcal{A} inherits the overall morphology from the Mandelbrot set, including the symmetry around the real axis. Furthermore, the following well-known regularities in which periodic cycles are organized within the Mandelbrot set³⁴ are preserved for \mathcal{A} . For c values in the main cardioid both f_c and F_c converge to fixed points. For the first main bulb positioned on the left side of the main cardioid, the dynamics are attracted by period-2 cycles. The subsequent bulb on the left has period-4. The upper-most and lower-most bulbs adjacent to the main cardioid are of period-3. To locate these period-3 bulbs, note that the upper ones are included in the dashed squares in Figs. 2(a) and 2(b). Starting from these period-3 bulbs and going rightward along the rim of the main cardioid, the locally largest bulbs are of period 4, 5, 6, and so on. On the left side of the period-3 bulbs, the locally largest bulbs have period 5, 7, 9, and so on. The periods of smaller bulbs on the rim of the main cardioid, which are not included in these sequences of locally largest bulbs, can be determined as follows. For any pair of bulbs, the period of the biggest bulb between them is given by the pair's sum of periods.

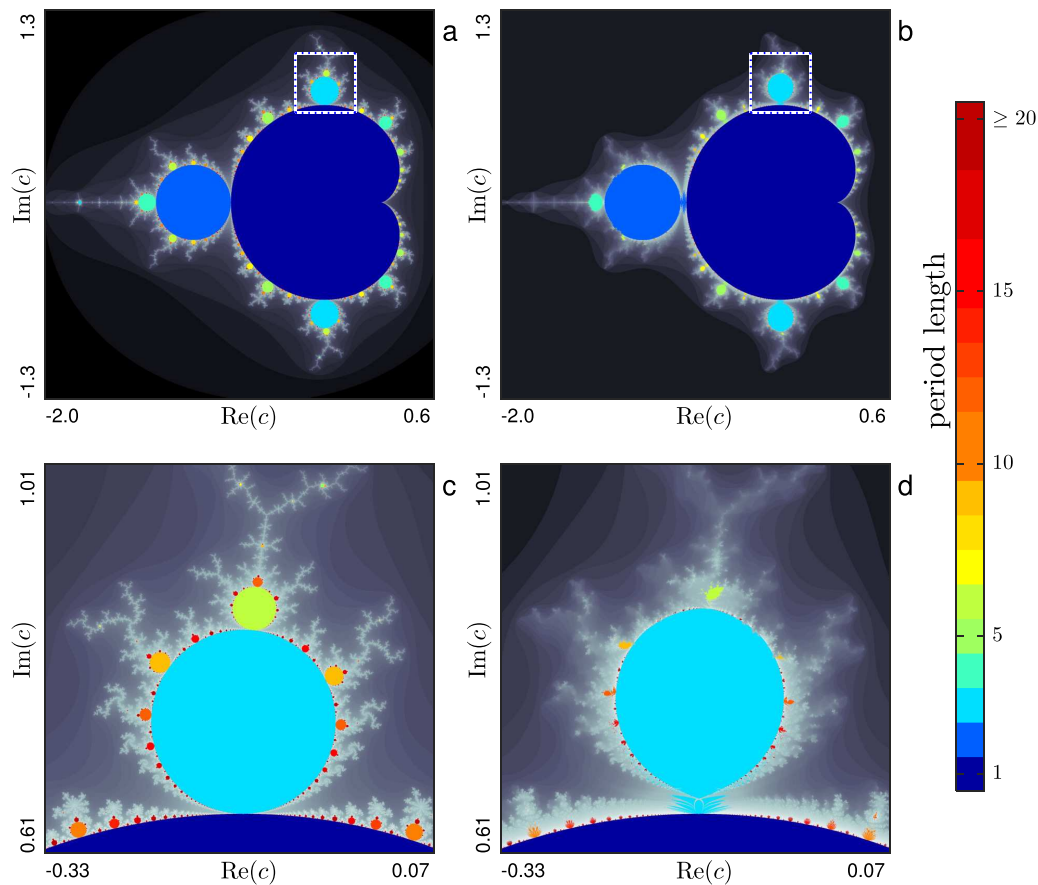


FIG. 2. The Mandelbrot set's overall morphology and spatial organization of periodic cycles is preserved in \mathcal{A} . (a) Gray areas: complement of the Mandelbrot set, i.e., the set of complex c for which the iterates of an individual quadratic map f_c diverge to infinity. The Mandelbrot set is given by the union of all non-gray areas. Inside the Mandelbrot set, the color indicates the period of the cycle into which the map f_c enters. (b) Gray areas: complement of the set \mathcal{A} , i.e., the set \mathcal{B} of complex c for which the iterates of the network of four coupled quadratic maps F_c diverge to infinity. Inside F_c , the color indicates the period of the cycle into which the network F_c enters. Panels (c) and (d) magnify the dashed squares in panels (a) and (b), respectively. In all panels, values of c are sampled on a regular 2000×2000 grid, and axis labels indicate values of the real and imaginary parts of c in the outermost corners. The gray scales are based on $\log_{10} n_{\text{div}}$, where lighter gray indicates higher n_{div} . The scales are adjusted for each panel to optimize the contrast.

Notwithstanding the aforementioned common overall morphology of \mathcal{A} and the Mandelbrot set, the bulbs of \mathcal{A} seem compressed, deformed, or missing altogether [Figs. 2(a) and 2(b)]. That these alterations do not only affect the shape of the bulbs becomes evident once we take a closer look at the upper principal period-3 bulb as an example [Figs. 2(c) and 2(d)]. For \mathcal{A} , the connection between this light blue bulb and the dark blue main cardioid is obstructed by gray ridges belonging to \mathcal{B} . Furthermore, pronounced changes are seen in the peripheral structure of the bulb. The filaments surrounding the bulb in the Mandelbrot set seem torn apart in \mathcal{A} . Does this mean that \mathcal{A} is merely a distorted and corrupted Mandelbrot set?

No. As can be seen from an iterative zoom across several orders of magnitude, this is not the case (Fig. 3). At all length scales in the complex plane, \mathcal{B} divides \mathcal{A} into smaller and smaller subsets. To describe this fragmentation, we coin the terminology of *ridges*

of instability, which separate *lakes of stability*. We can observe that each lake of stability contains c values leading to exclusively one of the five states of synchronization. Sometimes apparently adjacent areas of different non-gray colors at one magnification in Fig. 3 might suggest that a lake of stability includes different types of synchronization. However, a further zoom always reveals that these areas of different colors are actually separated by ridges of instability and, therefore, belong to different lakes of stability. In their entirety, the lakes of stability constitute \mathcal{A} . The ridges of instability belong to \mathcal{B} , which furthermore includes the overall enclosure of \mathcal{A} . In analogy to what we observe for the upper principal period-3 bulb in Fig. 2(d), we see in Figs. 3(b) and 3(c) that the connections between the main cardioid and higher-period bulbs are obstructed by ridges of instability. We use the upper-left period-5 bulb as example to zoom into smaller and smaller length scales in Figs. 3(c)–3(h). One can appreciate that the boundaries between instability ridges

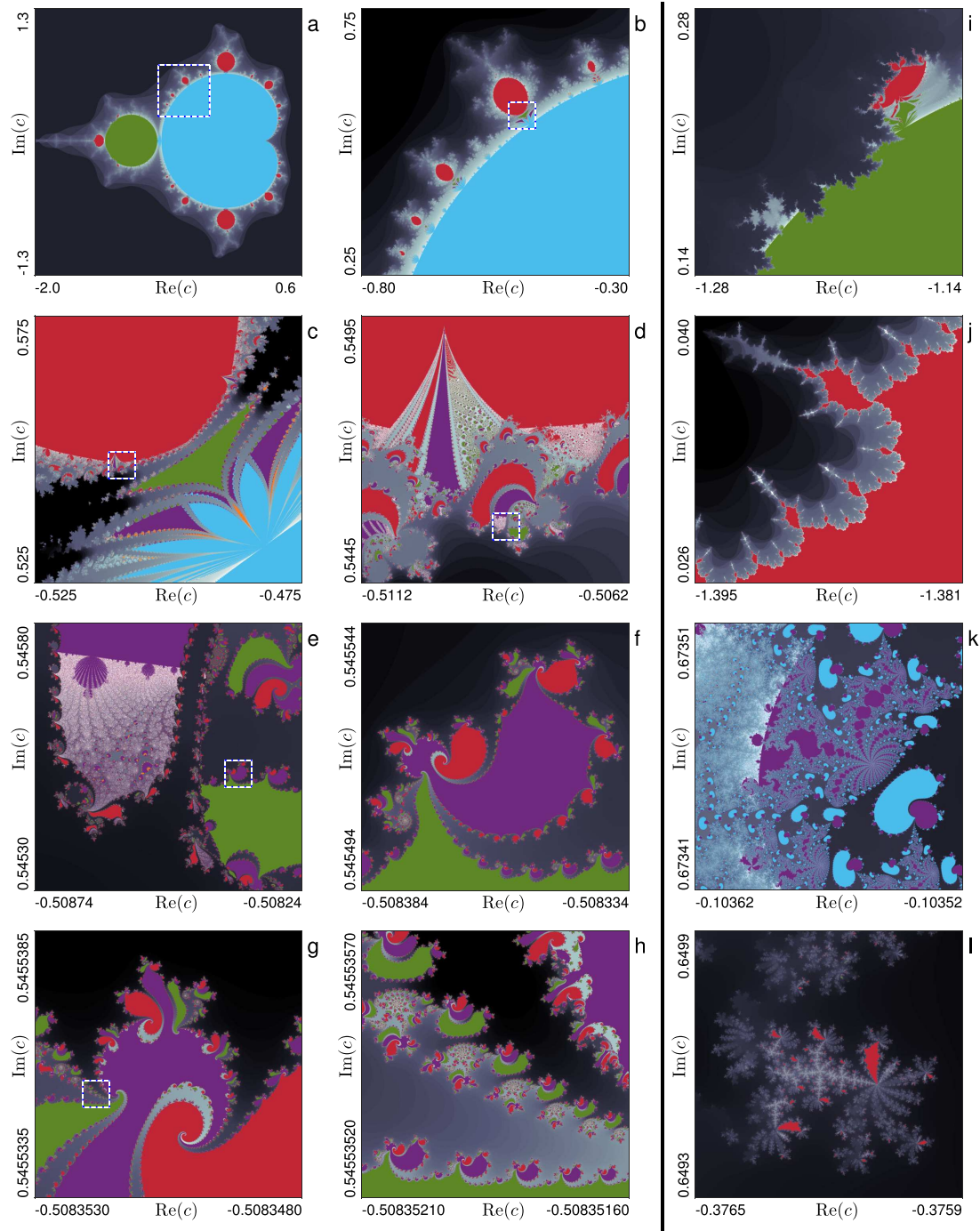


FIG. 3. Vadim's flowers and strawberry fields. In all panels, gray colors show the set \mathcal{B} , i.e., the set of complex c for which the iterates of the network of four coupled quadratic maps F_c diverge. Values of c constituting \mathcal{A} are depicted in different non-gray colors, each of which corresponds to a different state of synchronization. Blue: full synchronization; red: full desynchronization; yellow: within-pair synchronization; green: cross-pair synchronization; purple: chimera state. Panels (b)–(h) are successive zooms, magnifying the dashed squares in the preceding panels (a)–(g). Except for the first step, all magnifications are tenfold. Panels (i)–(l) show a selection of further patterns which in this case are not successive zooms. In all panels, values of c are sampled on a regular 2000×2000 grid, and axes labels indicate values of the real and imaginary part of c in the outermost corners. The gray scales are based on $\log_{10}(n_{div})$, where lighter gray indicates higher n_{div} . The scales are adjusted for each panel to optimize the contrast. All panels are magnified in Figs. 1–12 in the [supplementary material](#).

and stability lakes are never simple lines. Instead, these boundaries form fractal patterns. While these patterns show some similarities across length scales, a rich repertoire of diverse shapes is found on different scales [Figs. 3(a)–3(h)] and at different sites in the complex plane [Figs. 3(i)–3(l)]. Patterns never seem to be replicated identically at different scales, and \mathcal{A} is, therefore, not strictly self-similar. In more qualitative terms, one may say that details of the set \mathcal{A} seem less filigree than those of the Mandelbrot set. On the other hand, \mathcal{A} seems to be even fuller of variety.

Oftentimes, ridges of instability resemble octopus tentacles [Figs. 3(c) and 3(e)–3(g)]. Two vertically oriented and comparably straight tentacle-like ridges enclose a purple lake in the upper left of Fig. 3(e). The lower part of this purple lake is filled by instabilities, which in turn are perforated by countless purple and yellow stability lakes. The light gray color dominating the upper part of these instabilities indicates that for these c values F_c undergoes particularly long transients before the iterates eventually diverge to infinity. In this light gray region, we furthermore see cavities that resemble the main bulbs of the Mandelbrot set. These bulbs are segregated by tentacle-like structures, which get thinner and thinner toward the connections of the bulbs with the major purple lake. A further peculiar phenomenon is seen at the rim of the main period-2 bulb [Fig. 3(i)]. The way in which the instabilities penetrate this bulb might be compared to a lava flow overrunning a coastline. This flow also buries most of the period-6 bulb adjacent to the main period-2 bulb in the upper right of Fig. 3(i). Similar instabilities enter the main period-4 bulb from its left side [Fig. 3(j)]. Here, stability lakes with a high degree of self-similarity are encapsulated by the instabilities. This region of \mathcal{A} is dominated by full desynchronization such that all stability lakes are depicted in red in Fig. 3(j).

In Fig. 3(k), our attention is at first caught by the pairs of bean-shaped blue and purple lakes of stability. Opposite to the blue lakes, we find fountains of rays. These rays contain the aforementioned pairs of blue and purple lakes of stability, which grow in size upon increasing distance from the fountain centers. At first glance, some pairs of bean-shaped blue and purple lakes seem to be completely surrounded by instability, isolating them from any other formation. A closer look, however, reveals that this is not the case. What appears to be the connections of blue and purple lakes is also the origin of a stream filled with lakes that are smaller compared to the lakes from which they originate from. These springs grow and unite with other springs, such that the part of \mathcal{A} displayed in Fig. 3(k) does not contain any discernible formations completely surrounded by instability. In other regions of \mathcal{A} , however, we do find isolated formations of lakes. Consider, for example, the groups close to the diagonal of Fig. 3(h). To localize these groups, note that four of them are included in their entirety in Fig. 3(h), while two and one extend beyond the left and right margin of this panel, respectively. Each formation is constituted by a multitude of lakes and can be delineated as a distinct group since it is completely enclosed by ridges of instability. Further examples of isolated groups can be seen in the dark gray regions in Fig. 3(c) and in the periphery of a period-8 bulb [Fig. 3(l)]. To the best of our observation, in none of these cases, there are channels of stability which would cross through the instability ridges to establish a connection to these isolated formations. Hence, the set \mathcal{A} is not connected, which distinguishes it from the

Mandelbrot set, which is known to be connected (see Ref. 54, and references therein).

After ruling out the global connectivity of \mathcal{A} , an important question remains. Are different lakes of stability connected locally? In particular, can we take a path in the complex plane leading from one type of synchronization to another one without passing across a ridge of instability? As a first part of the answer, we note that we never observe line-shaped boundaries with zero broadness and non-zero length, which would separate areas formed by c values leading to different types of synchronization. Based on this observation, we conclude that each lake of synchronization contains only c values leading to exclusively one state of synchronization. However, connections between stability lakes might be established at points. To address this question, we take a closer look at swirls, examples of which can already be seen in Fig. 3. To analyze these swirls in more detail, we start in Fig. 4(a) with an example taken from the boundary of the main period-2 bulb of \mathcal{A} , and continue with iterative zooms into a prominent swirl of four tentacle-like instability ridges [Figs. 4(b)–4(d)]. Swirls of seven ridges are enclosed between two of the major ridges. Like indicated in the context of Fig. 3(j), this region of \mathcal{A} is dominated by full desynchronization. Therefore, the stability lakes in Figs. 4(a)–4(d) are depicted in red. This is different in the example shown in Figs. 4(e)–4(h), which is taken from the border of an instability ridge at the entrance of the main period-3 bulb of \mathcal{A} . Here, two stability lakes containing c values leading to within-pair synchronization and one stability lake containing c values leading to full synchronization jointly spiral into the swirl center. Furthermore, a magnification into one of the separating instability ridges reveals stability lakes of chimera states [Fig. 4(i)].

What is in the center of such swirls? To address this question for \mathcal{A} , we at first briefly look back at the Mandelbrot set. An example for a spiral-shaped swirl in the Mandelbrot set is shown in Figs. 4(j)–4(l). The periphery of the Mandelbrot set contains countless miniature approximate copies of itself [Fig. 4(j)]. However, no such miniature Mandelbrot set is located in the swirl center. Due to the asymptotic self-similarity at the center of the spiral, successive zooms solely seem to result in a rotation. No matter how much one increases the zoom, one would continue to see the same self-similar spiral. The center cannot be resolved.⁵⁵ Nonetheless, since the Mandelbrot set is connected, we know that the swirl center must belong to the Mandelbrot set. Otherwise, it would be impossible to pass from one spiral arm to the other, which would contradict with the set's connectedness. We conjecture that also the swirl centers in \mathcal{A} are point-like. In other words, we assume that they are not formed by a stability lake or instability ridge of non-zero area. However, for \mathcal{A} , we cannot use connectedness to conclude to the nature of this point. The swirl centers can belong to \mathcal{A} or to \mathcal{B} . One might speculate that this depends on whether or not all lakes of stability which approach a particular swirl center are of the same type of synchronization. If they all are of the same type, such as in Figs. 4(a)–4(d), the swirl center might belong to \mathcal{A} and show that same type of synchronization. If the lakes contain different types of synchronization, such as in Figs. 4(e)–4(h), they might be separated by the swirl center belonging to \mathcal{B} . However, these remain conjectures, and a definite answer as to whether swirl centers can be used to pass from one type of synchronization to another without leaving \mathcal{A} is left for future studies.

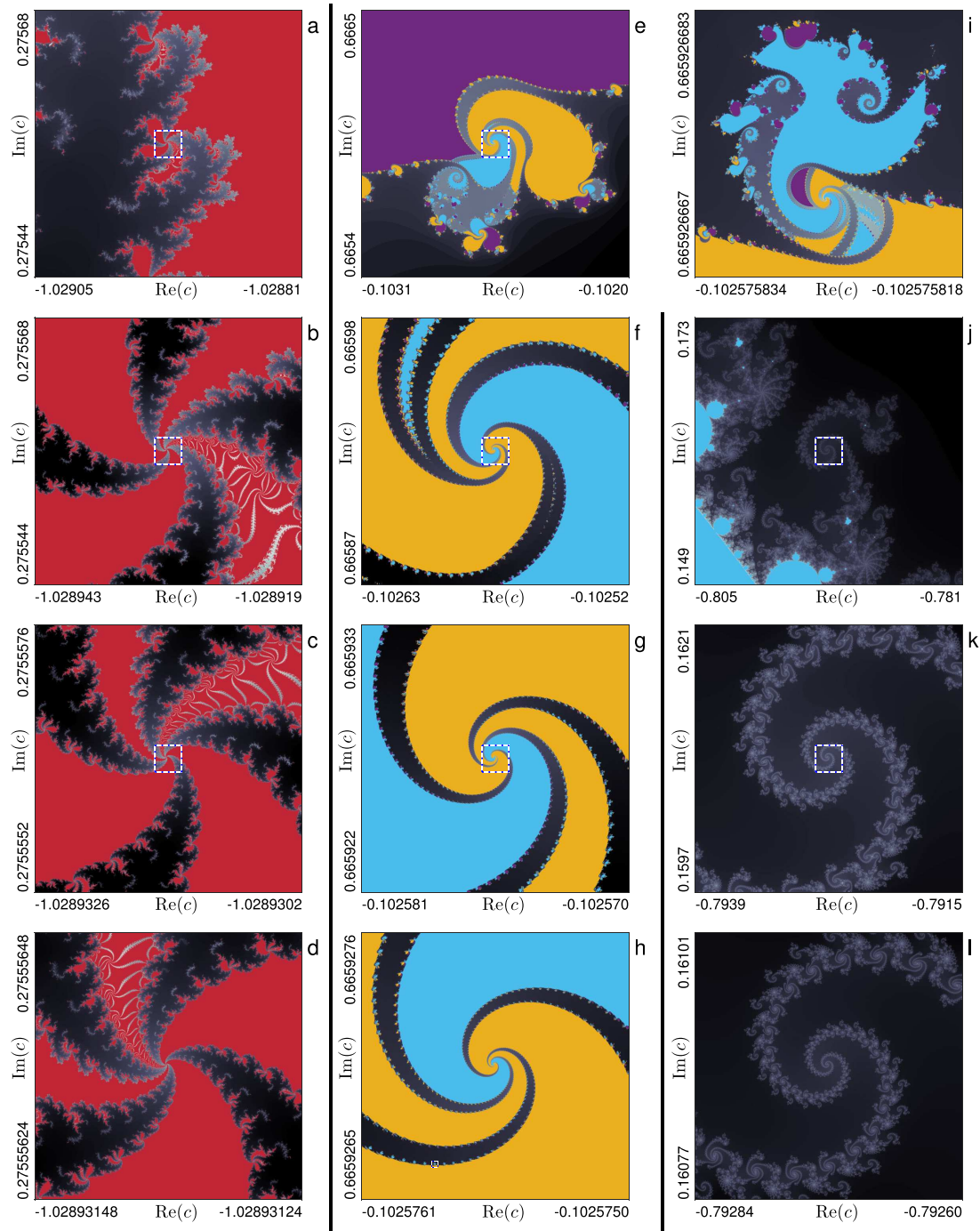


FIG. 4. Octopus's garden. (a)–(d) Same as Fig. 3, here highlighting a spiral-shaped swirl in \mathcal{A} . Panels (b)–(d) are successive tenfold zooms, magnifying the dashed squares in the preceding panels (a)–(c). Recall that the gray scales are adjusted for each panel to optimize the contrast. Without this adjustment, the instability ridges in panel (d) would be entirely light gray. (e)–(h) Same as panels (a)–(d), here showing a further example for a swirl. Panel (i) shows a magnification of the square in panel (h), corresponding to a 69-fold zoom. (j)–(l) Analogous to (a)–(h) showing a swirl for the Mandelbrot set. Accordingly, while panels (a)–(h) show results for the network of four coupled quadratic maps F_c , panels (j)–(l) are obtained for an individual quadratic map f_c . Graphs are drawn like in Figs. 2(a) and 2(c) but without distinguishing periodicity. Instead, all c values belonging to the Mandelbrot are plotted in blue. All panels are magnified in Figs. 13–24 in the supplementary material.

V. THE PECULIARITY OF THE REAL AXIS

The dynamics of F_c for parameters taken from the real axis, i.e., $c \in \mathbb{R}$, merit additional consideration (Fig. 5). First, we recall that the Mandelbrot set as well as \mathcal{A} are symmetric around the real axis and we note that both include the interval $\mathcal{I} = [-2, 0.25] \subset \mathbb{R}$ [see again Figs. 2(a) and 2(b)]. For all $c \in \mathcal{I}$, both f_c and F_c show bounded behavior, whereas they both diverge for all c , which are real-valued but outside of \mathcal{I} . At the interval limits $c = -2$ and $c = 0.25$, the map f_c converges to the fixed points 2 and 0.5, respectively. The network shows the same behavior, and all four maps converge to 2 for $F_{c=-2}$, and to 0.5 for $F_{c=0.25}$. In consequence, at both limits of \mathcal{I} , the network F_c enters into a fully synchronized state. Across the $c \in \mathcal{I}$, F_c attains all five states of synchronization (Fig. 5). Hence, all lakes of stability, which include subintervals of \mathcal{I} are connected via the points at the limits of their respective subintervals. Therefore, going along \mathcal{I} , it is possible to switch between all states of synchronization without crossing any ridge of instability. While we cannot answer yet whether swirl centers can be used to pass from one type of synchronization to another without leaving \mathcal{A} , we see that this passage is possible taking the simple path offered by \mathcal{I} .

A further important aspect is the existence of bounded aperiodic solutions of F_c for some of the $c \in \mathcal{I}$. It is known that decreasing the parameter c along \mathcal{I} , leads to a period-doubling bifurcation scenario for the individual map f_c . In Fig. 5, we use the example of U_c to show that the maps still exhibit a bifurcation scenario also when they are coupled to form the network F_c . Their bifurcation diagrams are different from the one of f_c , and the diagrams' fine structure depends on the coupling values C_w and C_a (see also Ref. 39). What matters here is that for $c \in \mathcal{I}$, we find both periodic and aperiodic solutions of F_c . For the coupling values used here, the fully desynchronized state, across-pair synchronization and chimera states are attained for both periodic and aperiodic dynamics. In contrast, the fully synchronized state and within-pair synchronization are only found in the periodic windows of the bifurcation diagram shown in Fig. 5.

Conversely, we found no evidence for bounded aperiodic solutions of F_c for any $c \notin \mathcal{I}$, i.e., for parameter values away from this subinterval of the real axis. Recall that for real-valued $c \notin \mathcal{I}$, the network always diverges to infinity. Very rarely, we found complex-valued $c \notin \mathcal{I}$ for which after n_{\max} iterations the network was still bounded and had not yet entered into any periodic cycle. However, detailed inspection of these particular cases always showed that transients were still ongoing. When we observed the dynamics beyond n_{\max} iterations, the transients continued along contracting or expanding patterns in the complex plane in a slow manner, suggesting that the dynamics would eventually settle down to a periodic cycle or diverge, respectively. A reliable distinction between long transients in bounded or diverging solutions, cycles of very high but finite period, and aperiodic solutions, if the latter exist for $c \notin \mathcal{I}$, will require a refined methodology and is left for future studies. Therefore, while Fig. 5 shows that $\mathcal{I} \subset \mathcal{A}$, and for some $c \in \mathcal{I}$, the network F_c shows bounded aperiodic dynamics, and we can only say that we found no evidence for such dynamics for parameters c with $c \in \mathcal{A}$ but $c \notin \mathcal{I}$.

VI. DISCUSSION AND OUTLOOK

The present study establishes a link between the dynamics of chimera states and the geometry of fractal structures in the complex plane. First links between chimeras and fractals were drawn already in Refs. 21–23. These studies showed that the set of initial conditions leading to chimeras^{21,22} or sub-chimeras²³ form riddled and fractal basins of attraction for networks of Rössler dynamics,²² Henon maps,²¹ logistic maps,²³ and sine-squared maps²³ (see also Ref. 56). The spaces of basins of attraction are high-dimensional, and one can only inspect projections to two dimensions. In contrast, our fractal set \mathcal{A} resides in the complex plain and can, therefore, readily be displayed and explored. We furthermore note that the term fractal is used to refer to certain hierarchical connectivity architectures

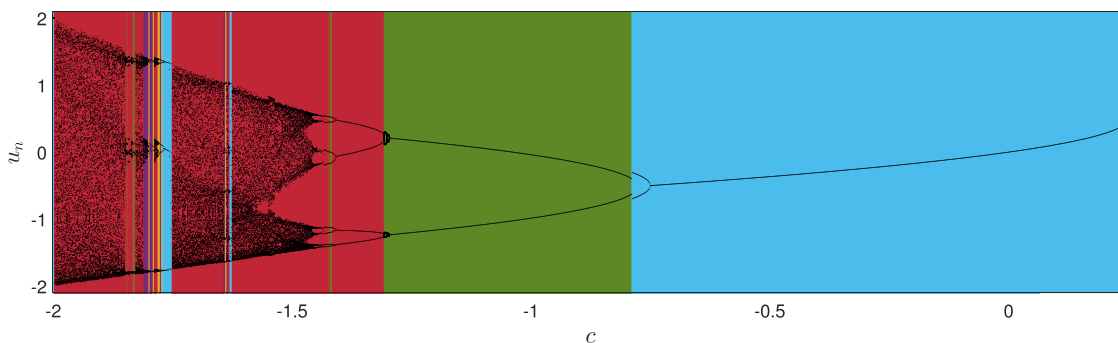


FIG. 5. Real-valued c leads to both periodic and aperiodic dynamics of the network of four coupled quadratic maps F_c covering all states of synchronization. Asymptotic states of u_n in dependence on c varied within \mathcal{I} in steps of 0.013 [same step size as in Figs. 2(a), 2(b) and 3(a)]. For c leading to a dynamics with period- m , dots show the m iterates constituting this cycle. Accordingly, dynamics of period m can be identified by m branches at the corresponding c value. In contrast, for c leading to aperiodic dynamics, the iterates are not constrained to such branches, and the dots show the last 100 iterates of u_n prior the n_{\max} -th iterate. The colors indicate which state of synchronization the network attains in dependence on c . Blue: full synchronization; yellow: within-pair synchronization; green: across-pair synchronization; purple: chimera state; red: full desynchronization (same color code as in Figs. 3–4). Analogous results to those shown here for U_c are obtained for the other three maps (not shown). At the right transition from full synchronization (blue) to across-pair synchronization (green), the fully synchronized period-2 motion of all four maps ($U_c = P_c = V_c = Q_c$) loses stability. Two distinct period-2 orbits (for example, $U_c = P_c \neq V_c = Q_c$) arise instead. This explains discontinuities at such transitions in this bifurcation diagram of U_c .

in networks generating chimera networks (e.g., Refs. 28 and 57–61). However, this notion of fractal connectivity is unrelated from the way in which the term fractal is used in Refs. 21–23 and in the present study. References 62 and 63 studied ring networks of N locally coupled quadratic maps for which the parameters c were varied independently for each map yielding a spatial Mandelbrot set of dimensionality $2N$. This high dimensionality again only allows one to inspect projections to subspaces, and Refs. 62 and 63 did not analyze the dynamics of the coupled maps with regard to their synchronization.

There are several important advances achieved by the present study with regard to our previous work,³⁹ in which we used two large populations of each 100 quadratic maps f_c . In the main part of Ref. 39, we studied the network's dynamics for a single real-valued $c = -1.8 \in \mathcal{I}$ using random real-valued initial conditions. Upon variation of the coupling strengths within and across populations, the network showed a plentitude of synchronous vs asynchronous, periodic vs aperiodic, and symmetric vs symmetry broken dynamics. It furthermore exhibited multistability by settling to distinct dynamics for different realizations of the initial conditions or by switching intermittently between distinct dynamics for the same realization. However, since we used a real-valued c and real-valued initial conditions, the network dynamics remained real-valued throughout the main part of Ref. 39. Only as a brief outlook, this previous work studied for which complex-valued c , the network iterates remained bounded or diverged. Results already showed that the capacity of the quadratic map f_c to generate fractal structures in the complex plane is inherited by networks of coupled quadratic maps. However, beyond the classification into bounded and divergent behavior, Ref. 39 paid no further attention to the network's dynamics. This is achieved in the present study, by detecting different states of synchronization of the network's iterates in the complex plane (see again Fig. 1 and Table 1). The most important finding, in our view, is that mapping the different states of synchronization of F_c as a function of its parameter c in the complex

plane leads to fractal structures with an additional level of complexity. The set \mathcal{A} , defined by the set of c for which F_c remains bounded, is divided into a presumably infinite number of subsets. We here coined the terms of lakes of stability, which are enclosed by ridges of instability. To the best of our observation, each lake contains exactly one state of synchronization (see again Figs. 3 and 4). Arbitrarily, small changes in c can be decisive for whether the network iterates diverge or remain bounded and determine whether bounded solutions get fully synchronized, fully desynchronized, or enter into some partially synchronized state, including a chimera state. Nonetheless, the only path in the complex plane for which we can confirm that it allows one to pass between all states of synchronization without crossing an instability is given by the real-valued $c \in \mathcal{I} = [-2, 0.25]$.

A further important difference between the present study and our previous work,³⁹ originates from the way in which we can define the initial conditions of these networks. In the main part of Ref. 39, which was solely dealing with real-valued dynamics, we followed earlier work of ours^{64–68} and used random initial conditions. However, as explained in the following, random initial conditions do not allow us to generate fractal structures in the complex plane. We at first briefly note that the c values forming the Mandelbrot set are all contained in the closed disk of radius 2 around the origin of the complex plane. For all c in this disk, the map $f_c(z_{n=0})$ diverges for $|z_{n=0}| > 2$. Therefore, any initial conditions $|z_{n=0}| > 2$ are directly discarded, and the following considerations are restricted to initial conditions $|z_{n=0}| \leq 2$. For a given value of c , it depends on $z_{n=0}$ whether the individual map f_c diverges or remains bounded. The boundaries between diverging and bounded behavior of f_c in the domain of complex-valued initial conditions $z_{n=0}$ defines Julia sets.^{40,41} In consequence, the question if the iterates of f_c or F_c remain bounded for a certain c , cannot be answered without specifying the initial conditions. That is the reason why the set \mathcal{A} , which is defined from the boundedness of F_c , cannot be defined for random initial conditions.

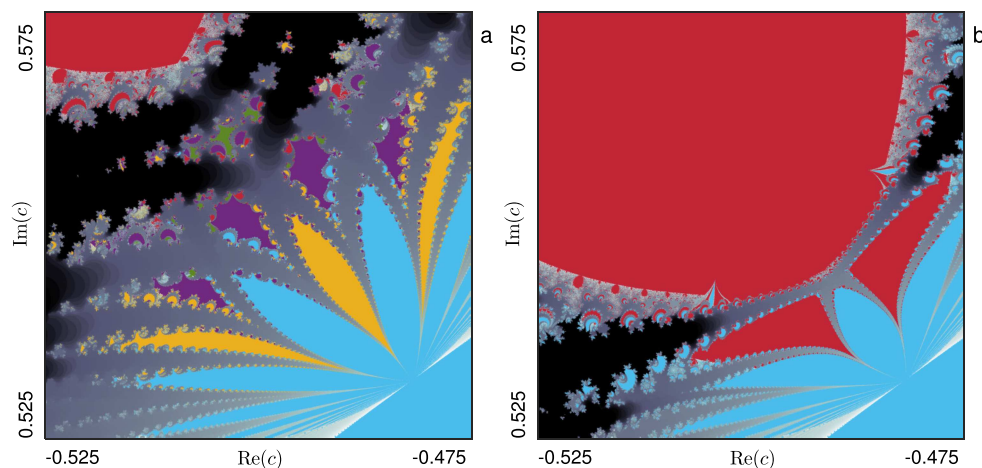


FIG. 6. Impact of coupling strengths and an even simpler network. (a) Same as Fig. 3(c) but here for $C_w = 0.02$ and $C_a = 0.0025$. Accordingly, panel (a) shows results for the network of four coupled quadratic maps F_c . Results shown in panel (b) are obtained for the same area as in (a) but for a network reduced to a single pair of two quadratic maps U_c and V_c coupled with $C_w = 0.01$. We observe synchronization $U_c = V_c$ (blue), desynchronization $U_c \neq V_c$ (red), or divergence to infinity (gray).

Our approach to use the first $2N$ iterates of the uncoupled map f_c started at $z_0 = 0$ as initial conditions for the two populations of each N maps is straightforward but remains of course somewhat arbitrary. In fact, for high N , it leads to a different problem. For many values of c outside of the Mandelbrot set, the map f_c diverges quickly and leaves the limits of floating point numbers after a few dozens of iterations. For these c values, it was, therefore, impossible to generate 200 finite-valued iterates to be used as initial conditions for the $2N = 200$ maps used in Ref. 39. For this reason, we restricted this previous study to c values inside the Mandelbrot set. By definition of this set, the map f_c never diverges for these c and initial conditions can, therefore, always be defined from the first 200 iterates. In consequence, in Ref. 39, we could only study the additional fractal structure generated inside the Mandelbrot set. Since we here only use four maps, this limitation does not apply. The iterates of f_c started at $z_{n=0} = 0$ never leave the limits of floating point numbers within the first $n = 4$ iterates. These first iterates can always be used as initial conditions for F_c . In the current study, we can, therefore, assess the full set \mathcal{A} without restricting it *a priori* to the inside of the Mandelbrot set.

We concluded in Ref. 39 that the high dimensionality of two populations of each 100 quadratic maps leads to the additional complexity in the fractal patterns described in this previous work. The present study, however, shows that this complexity is already observed for the minimal two-population network of two pairs of two quadratic maps. In fact, upon variation of the coupling strengths we can generate a whole family of fractal sets $\mathcal{A}(C_w, C_a)$. As one example, in Fig. 6(a), we revisit the area already inspected in Fig. 3(c) but now using $C_w = 0.02$ and $C_a = 0.0025$ instead of $C_w = 0.01$ and $C_a = 0.0025$. The change of the coupling strengths leads to a major reshaping of the instability ridges and enclosed stability lakes. A study of the coupling strengths' influence should also test for the existence of across-pair chimera states (e.g., $U_c = P_c \neq V_c \neq Q_c \neq U_c$) or triplet-singlet states⁴⁸ (e.g., $U_c = P_c = V_c \neq Q_c$).

Can we observe fractal boundaries of synchronization for even smaller networks? Yes, as we can see in Fig. 6(b), a single pair of two coupled quadratic maps is already sufficient. To illustrate this, we set $C_w = 0.01$ and $C_a = 0$ such that the network F_c falls apart into two mutually independent pairs of maps, of which we consider only the pair U_c and V_c . Since we have only two maps, there are only two possible bounded states. Either the two maps synchronize or they do not [Fig. 6(b)]. Despite this reduction in the diversity of the dynamics, the fractal patterns generated by just two maps seem of similar complexity as the ones generated by two pairs of two maps.

SUPPLEMENTARY MATERIAL

See the [supplementary material](#) consisting of Figs. 1–12 for enlarged displays of the 12 panels of Fig. 3 and Figs. 13–24 for enlarged displays of the 12 panels of Fig. 4.

DEDICATION

This work is dedicated to the late Vadim Anishchenko.

ACKNOWLEDGMENTS

We are grateful to Anaïs Espinosa, Christian Rummel, and Yuanzhao Zhang for useful discussions on the manuscript.

APPENDIX: PARAMETER VALUES USED FOR FIG. 1

TABLE II. Values of the parameter c used to generate the examples shown in Fig. 1 with the respective panel indicated in the last column. We specify the values with eight significant digits. Since arbitrarily small changes of c can lead to a qualitatively different asymptotic dynamics, one needs the exact values at double floating point precision to reproduce Fig. 1. These values are provided along with the source codes to run our computations at the electronic library repository of the Universitat Pompeu Fabra.⁶⁹

#	Value	Fig. 1
c_1	$-0.255\ 505\ 51 + 0.633\ 283\ 28i$	(a)
c_2	$-0.114\ 314\ 31 + 0.656\ 056\ 06i$	(b)
c_3	$-0.129\ 729\ 73 + 0.655\ 005\ 01i$	(c)
c_4	$-0.117\ 467\ 47 + 0.663\ 063\ 06i$	(d)
c_5	$-0.106\ 659\ 59 + 0.672\ 613\ 59i$	(e)
c_6	$-0.111\ 161\ 16 + 0.673\ 923\ 92i$	(f)
c_7	$+0.375\ 795\ 80 + 0.178\ 228\ 23i$	(g)
c_8	$-0.106\ 659\ 59 + 0.672\ 613\ 49i$	(h)

DATA AVAILABILITY

The data that support the findings of this study are openly available in the electronic library repository of the Universitat Pompeu Fabra (<https://repositori.upf.edu/>) at <https://doi.org/10.34810/data49>, Ref. 69.

REFERENCES

- V. V. Astakhov, V. S. Anishchenko, and A. V. Shabunin, "Controlling spatiotemporal chaos in a chain of the coupled logistic maps," *IEEE Trans. Circuits Syst. I: Fundam. Theor. Appl.* **42**, 352–357 (1995).
- V. S. Anishchenko, T. E. Vadivasova, G. I. Strelkova, and A. S. Kopeikin, "Chaotic attractors of two-dimensional invertible maps," *Discrete Dyn. Nat. Soc.* **2**, 249–256 (1998).
- V. Astakhov, A. Shabunin, A. Klimshin, and V. Anishchenko, "In-phase and antiphase complete chaotic synchronization in symmetrically coupled discrete maps," *Discrete Dyn. Nat. Soc.* **7**, 215–229 (2002).
- T. E. Vadivasova, G. I. Strelkova, S. A. Bogomolov, and V. S. Anishchenko, "Correlation analysis of the coherence–incoherence transition in a ring of nonlocally coupled logistic maps," *Chaos* **26**, 093108 (2016).
- S. Bogomolov, G. Strelkova, E. Schöll, and V. Anishchenko, "Amplitude and phase chimeras in an ensemble of chaotic oscillators," *Tech. Phys. Lett.* **42**, 765–768 (2016).
- S. A. Bogomolov, A. V. Slepnev, G. I. Strelkova, E. Schöll, and V. S. Anishchenko, "Mechanisms of appearance of amplitude and phase chimera states in ensembles of nonlocally coupled chaotic systems," *Commun. Nonlinear Sci. Numer. Simul.* **43**, 25–36 (2017).
- G. I. Strelkova, T. E. Vadivasova, and V. S. Anishchenko, "Synchronization of chimera states in a network of many unidirectionally coupled layers of discrete maps," *Regul. Chaotic Dyn.* **23**, 948–960 (2018).
- E. Rybalova, T. Vadivasova, G. Strelkova, V. Anishchenko, and A. Zakharova, "Forced synchronization of a multilayer heterogeneous network of chaotic maps in the chimera state mode," *Chaos* **29**, 033134 (2019).
- M. Winkler, J. Sawicki, I. Omelchenko, A. Zakharova, V. Anishchenko, and E. Schöll, "Relay synchronization in multiplex networks of discrete maps," *Europhys. Lett.* **126**, 50004 (2019).
- N. Semenova, A. Zakharova, E. Schöll, and V. Anishchenko, "Does hyperbolicity impede emergence of chimera states in networks of nonlocally coupled chaotic oscillators?," *Europhys. Lett.* **112**, 40002 (2015).

- ¹¹N. I. Semenova, E. V. Rybalova, G. I. Strelkova, and V. S. Anishchenko, “Coherence–incoherence” transition in ensembles of nonlocally coupled chaotic oscillators with nonhyperbolic and hyperbolic attractors,” *Regul. Chaotic Dyn.* **22**, 148–162 (2017).
- ¹²N. Semenova, G. Strelkova, V. Anishchenko, and A. Zakharova, “Temporal intermittency and the lifetime of chimera states in ensembles of nonlocally coupled chaotic oscillators,” *Chaos* **27**, 061102 (2017).
- ¹³A. Bukh, E. Rybalova, N. Semenova, G. Strelkova, and V. Anishchenko, “New type of chimera and mutual synchronization of spatiotemporal structures in two coupled ensembles of nonlocally interacting chaotic maps,” *Chaos* **27**, 111102 (2017).
- ¹⁴E. Rybalova, G. Strelkova, E. Schöll, and V. Anishchenko, “Relay and complete synchronization in heterogeneous multiplex networks of chaotic maps,” *Chaos* **30**, 061104 (2020).
- ¹⁵E. Rybalova, G. Strelkova, and V. Anishchenko, “Impact of sparse inter-layer coupling on the dynamics of a heterogeneous multilayer network of chaotic maps,” *Chaos, Solitons Fract.* **142**, 110477 (2021).
- ¹⁶I. A. Shepelev, A. V. Bukh, G. I. Strelkova, T. E. Vadivasova, and V. S. Anishchenko, “Chimera states in ensembles of bistable elements with regular and chaotic dynamics,” *Nonlinear Dyn.* **90**, 2317–2330 (2017).
- ¹⁷I. A. Shepelev, A. Bukh, T. E. Vadivasova, V. S. Anishchenko, and A. Zakharova, “Double-well chimeras in 2d lattice of chaotic bistable elements,” *Commun. Nonlinear Sci. Numer. Simul.* **54**, 50–61 (2018).
- ¹⁸A. Bukh, E. Schöll, and V. Anishchenko, “Synchronization of spiral wave patterns in two-layer 2D lattices of nonlocally coupled discrete oscillators,” *Chaos* **29**, 053105 (2019).
- ¹⁹Y. Kuramoto and D. Battogtokh, “Coexistence of coherence and incoherence in nonlocally coupled phase oscillators,” *Nonlinear Phenom. Complex Syst.* **5**, 380–385 (2002).
- ²⁰D. M. Abrams and S. H. Strogatz, “Chimera states for coupled oscillators,” *Phys. Rev. Lett.* **93**, 174102 (2004).
- ²¹V. Santos, J. D. Szezech, A. M. Batista, K. C. Iarosz, M. S. Baptista, H. P. Ren, C. Grebogi, R. L. Viana, I. L. Caldas, Y. L. Maistrenko, and J. Kurths, “Riddling: Chimera’s dilemma,” *Chaos* **28**, 081105 (2018).
- ²²V. dos Santos, F. S. Borges, K. C. Iarosz, I. L. Caldas, J. Szezech, R. L. Viana, M. S. Baptista, and A. M. Batista, “Basin of attraction for chimera states in a network of Rössler oscillators,” *Chaos* **30**, 083115 (2020).
- ²³Y. Zhang, Z. G. Nicolaou, J. D. Hart, R. Roy, and A. E. Motter, “Critical switching in globally attractive chimeras,” *Phys. Rev. X* **10**, 011044 (2020).
- ²⁴I. Omelchenko, Y. Maistrenko, P. Hövel, and E. Schöll, “Loss of coherence in dynamical networks: Spatial chaos and chimera states,” *Phys. Rev. Lett.* **106**, 234102 (2011).
- ²⁵I. Omelchenko, B. Riemenschneider, P. Hövel, Y. Maistrenko, and E. Schöll, “Transition from spatial coherence to incoherence in coupled chaotic systems,” *Phys. Rev. E* **85**, 026212 (2012).
- ²⁶Y. Zhang and A. E. Motter, “Mechanism for strong chimeras,” *Phys. Rev. Lett.* **126**(9), 094101 (2021).
- ²⁷I. Korneev, V. Semenov, A. Slepnev, and T. Vadivasova, “Complete synchronization of chaos in systems with nonlinear inertial coupling,” *Chaos, Solitons Fract.* **142**, 110459 (2021).
- ²⁸A. zur Bonsen, I. Omelchenko, A. Zakharova, and E. Schöll, “Chimera states in networks of logistic maps with hierarchical connectivities,” *Eur. Phys. J. B* **91**, 65 (2018).
- ²⁹S. Ghosh, A. Zakharova, and S. Jalan, “Non-identical multiplexing promotes chimera states,” *Chaos, Solitons Fract.* **106**, 56–60 (2018).
- ³⁰P. Chandran, R. Gopal, V. Chandrasekar, and N. Athavan, “Chimera states in coupled logistic maps with additional weak nonlocal topology,” *Chaos* **29**, 053125 (2019).
- ³¹T. Vadivasova, A. Slepnev, and A. Zakharova, “Control of inter-layer synchronization by multiplexing noise,” *Chaos* **30**, 091101 (2020).
- ³²L. Khaleghi, S. Panahi, S. N. Chowdhury, S. Bogomolov, D. Ghosh, and S. Jafari, “Chimera states in a ring of map-based neurons,” *Physica A* **536**, 122596 (2019).
- ³³C. R. Nayak and N. Gupte, “Chimera states in coupled sine-circle map lattices,” *AIP Conf. Proc.* **1339**, 172–180 (2011).
- ³⁴J. Singha and N. Gupte, “Spatial splay states and splay chimera states in coupled map lattices,” *Phys. Rev. E* **94**, 052204 (2016).
- ³⁵J. Singha and N. Gupte, “Chimera states in coupled map lattices: Spatiotemporally intermittent behavior and an equivalent cellular automaton,” *Chaos* **30**, 113102 (2020).
- ³⁶J. D. Hart, D. C. Schmadel, T. E. Murphy, and R. Roy, “Experiments with arbitrary networks in time-multiplexed delay systems,” *Chaos* **27**, 121103 (2017).
- ³⁷A. M. Hagerstrom, T. E. Murphy, R. Roy, P. Hövel, I. Omelchenko, and E. Schöll, “Experimental observation of chimeras in coupled-map lattices,” *Nat. Phys.* **8**, 658–661 (2012).
- ³⁸D. Dudkowski, Y. Maistrenko, and T. Kapitaniak, “Different types of chimera states: An interplay between spatial and dynamical chaos,” *Phys. Rev. E* **90**, 032920 (2014).
- ³⁹R. G. Andrzejak, G. Ruzzene, E. Schöll, and I. Omelchenko, “Two populations of coupled quadratic maps exhibit a plentitude of symmetric and symmetry broken dynamics,” *Chaos* **30**, 033125 (2020).
- ⁴⁰P. Fatou, “Sur les substitutions rationnelles,” *C. R. Acad. Sci. Paris* **164**, 806–808 (1917).
- ⁴¹G. Julia, “Mémoire sur la permutabilité des fractions rationnelles,” in *Annales Scientifiques de l’École Normale Supérieure* (Numdam, 1922), Vol. 39, pp. 131–215.
- ⁴²R. Brooks and J. P. Matelski, “The dynamics of 2-generator subgroups of PSL(2, C),” in *Riemann Surfaces and Related Topics: Proceedings of the 1978 Stony Brook Conference*, *Annals of Mathematics Studies* Vol. 97 (1981), pp. 65–71.
- ⁴³B. B. Mandelbrot, “Fractal aspects of the iteration of $z\lambda z(1-z)$ for complex λ and z ,” *Ann. N. Y. Acad. Sci.* **357**, 249–259 (1980).
- ⁴⁴A. Douady, J. H. Hubbard, and P. Lavaurs, “Etude dynamique des polynômes complexes,” *Publ. Math. Orsay* **2**, 4 (1984).
- ⁴⁵P. Ashwin and O. Burylko, “Weak chimeras in minimal networks of coupled phase oscillators,” *Chaos* **25**, 013106 (2015).
- ⁴⁶F. Böhm, A. Zakharova, E. Schöll, and K. Lüdge, “Amplitude-phase coupling drives chimera states in globally coupled laser networks,” *Phys. Rev. E* **91**, 040901 (2015).
- ⁴⁷M. J. Panaggio, D. M. Abrams, P. Ashwin, and C. R. Laing, “Chimera states in networks of phase oscillators: The case of two small populations,” *Phys. Rev. E* **93**, 012218 (2016).
- ⁴⁸J. D. Hart, K. Bansal, T. E. Murphy, and R. Roy, “Experimental observation of chimera and cluster states in a minimal globally coupled network,” *Chaos* **26**, 094801 (2016).
- ⁴⁹J. Wojewoda, K. Czolczynski, Y. Maistrenko, and T. Kapitaniak, “The smallest chimera state for coupled pendula,” *Sci. Rep.* **6**, 34329 (2016).
- ⁵⁰Y. Maistrenko, S. Brezetsky, P. Jaros, R. Levchenko, and T. Kapitaniak, “Smallest chimera states,” *Phys. Rev. E* **95**, 010203 (2017).
- ⁵¹P. Ebrahimzadeh, M. Schiek, P. Jaros, T. Kapitaniak, S. van Waasen, and Y. Maistrenko, “Minimal chimera states in phase-lag coupled mechanical oscillators,” *Eur. Phys. J. Spec. Top.* **229**, 2205–2214 (2020).
- ⁵²J. Sharma, I. Tiwari, D. Das, and P. Parmananda, “Chimeralike states in a minimal network of active camphor ribbons,” *Phys. Rev. E* **103**, 012214 (2021).
- ⁵³We performed the analysis using MATLAB with double floating point precision. The values of the quadratic map are of the order 10^0 . The value ϵ_{NUM} is, therefore, just above the resolution of the double floating point precision.⁵⁰ Pre-analysis showed this threshold to be optimal in minimizing the impact of numerical roundoff errors.
- ⁵⁴H.-O. Peitgen, H. Jürgens, and D. Saupe, *Chaos and Fractals: New Frontiers of Science* (Springer Science & Business Media, 2006).
- ⁵⁵For a more detailed discussion of these spirals in the Mandelbrot set, their relation to the corresponding Julia sets, and Misiurewicz points, see Ref. 54, and references therein.
- ⁵⁶E. A. Martens, M. J. Panaggio, and D. M. Abrams, “Basins of attraction for chimera states,” *New J. Phys.* **18**, 022002 (2016).
- ⁵⁷J. Hizanidis, E. Panagakou, I. Omelchenko, E. Schöll, P. Hövel, and A. Provata, “Chimera states in population dynamics: Networks with fragmented and hierarchical connectivities,” *Phys. Rev. E* **92**, 012915 (2015).
- ⁵⁸S. Ulonska, I. Omelchenko, A. Zakharova, and E. Schöll, “Chimera states in networks of Van der Pol oscillators with hierarchical connectivities,” *Chaos* **26**, 094825 (2016).

- ⁵⁹J. Sawicki, I. Omelchenko, A. Zakharova, and E. Schöll, “Chimera states in complex networks: Interplay of fractal topology and delay,” *Eur. Phys. J. Spec. Top.* **226**, 1883–1892 (2017).
- ⁶⁰T. Chouzouris, I. Omelchenko, A. Zakharova, J. Hlinka, P. Jiruska, and E. Schöll, “Chimera states in brain networks: Empirical neural vs. modular fractal connectivity,” *Chaos* **28**, 045112 (2018).
- ⁶¹G. Argyropoulos and A. Provata, “Chimera states with 2D deterministic and random fractal connectivity,” *Front. Appl. Math. Stat.* **5**, 35 (2019).
- ⁶²P. Liu, “Control and synchronization of Mandelbrot sets in coupled map lattice,” *Nonlinear Dyn.* **73**, 299–310 (2013).
- ⁶³D. Wang, S. Liu, Y. Zhao, and C. Jiang, “Control of the spatial Mandelbrot set generated in coupled map lattice,” *Nonlinear Dyn.* **84**, 1795–1803 (2016).
- ⁶⁴R. G. Andrzejak, C. Rummel, F. Mormann, and K. Schindler, “All together now: Analogies between chimera state collapses and epileptic seizures,” *Sci. Rep.* **6**, 23000 (2016).
- ⁶⁵R. G. Andrzejak, G. Ruzzene, and I. Malvestio, “Generalized synchronization between chimera states,” *Chaos* **27**, 053114 (2017).
- ⁶⁶R. G. Andrzejak, G. Ruzzene, I. Malvestio, K. Schindler, E. Schöll, and A. Zakharova, “Mean field phase synchronization between chimera states,” *Chaos* **28**, 091101 (2018).
- ⁶⁷G. Ruzzene, I. Omelchenko, E. Schöll, A. Zakharova, and R. G. Andrzejak, “Controlling chimera states via minimal coupling modification,” *Chaos* **29**, 051103 (2019).
- ⁶⁸G. Ruzzene, I. Omelchenko, J. Sawicki, A. Zakharova, E. Schöll, and R. G. Andrzejak, “Remote pacemaker control of chimera states in multilayer networks of neurons,” *Phys. Rev. E* **102**, 052216 (2020).
- ⁶⁹Open access library repository, Universitat Pompeu Fabra, <https://doi.org/10.34810/data49>.
- ⁷⁰IEEE Standards Committee, “754-2008 IEEE standard for floating-point arithmetic,” IEEE Comput. Soc. Std. 1–70 (2008).